ISSN No:-2456-2165

Temporal Variation in Water Column Structure in Southampton Water during a Partial Tidal Cycle

Michael L. Hackett
Department of Mathematics,
Physics & Statistics, University of Guyana,
Tain Campus, Guyana

Ashmini Prasad
Tagore Memorial Secondary School,
Ministry of Education,
Guyana

Abstract:- This research investigates the temporal variation in the water column structure during a partial tidal cycle in the Western Solent at a location just off the mouth of the Beaulieu River. The data were collected using the Acoustic Doppler Current Profiler, the Conductivity-Temperature-Depth instrument, and the Autonomous Benthic Recorder. The properties of the water column structure investigated were temperature, salinity, flow velocity, and turbidity at different depths during the partial tidal cycle. It will be shown that these identified properties of the water column vary temporally and spatially in the vertical during the partial tidal cycle. Relationships will be demonstrated among these properties to show that their variations are caused mainly by the ebb and flow of the tidal cycle which dynamically influences the structure of the water column in time and space.

Keywords:- *Water column, turbidity, velocity profile, shear stress, ebb tide, flood tide, temperature, salinity, stratification, suspended sediments, vertical mixing, acoustic Doppler current profiler (ACDC), conductivity-temperature depth instrument (CTD).*

I. INTRODUCTION

The water column in nature is not just a homogeneous column of water with invariable properties throughout, as observed in a body of undisturbed distilled water in a laboratory; instead, there are variations of the properties of the water column in the vertical. Tides may cause these variations: prevailing winds, waves, solar radiation, exchange of water with other sources, and the presence of soluble and insoluble substances.

For instance, any solute in water will cause its density to increase so that the greater the amount of solute, the greater the density. This has the effect of lowering both the freezing point of water and its maximum-density temperature so that its density is controlled only by thermal expansion (Oceanography Course Team, 1989). So, when the water column absorbs thermal solar energy, the warmer, less dense water is situated above the colder, denser water, producing a stratification of the water column with respect to temperature and salinity. However, due to the time-varying phenomena of tides, winds, waves, and run-offs from freshwater sources, vertical mixing processes are set up that cause the stratification of the water column to vary over time (Dyer, 1973), hence the term 'temporal variation'.

Turbidity is caused by the presence of suspended sediments, such as mud and sand, in the water column. These sediments were displaced from the bed and sent into suspension by turbulence generated by bed shear stresses produced as water flows over the bed. The turbulence also contributes to the mixing processes in the water column (Open University Course Team, 1989). Due to the changes in the flow velocity of water during the tidal cycle, we would expect to see a variation of turbidity through the water column, and because the flow velocity is depth dependent (Yalin, 1972; Nielsen, 1992), we would also expect turbidity to vary with depth.

This research attempts to understand the relations, patterns, and trends that exist among the parameters that make up the water column structure during the partial tidal cycle.

II. MATERIALS & METHOD

The data for this research were collected on March 6, 2009 (10:10 – 15:10 hours UT), about 1 km north of the mouth of the Beaulieu River in the Western Solent on the coastal vessel R.V. Bill Conway. The water depth was approximately 5m. Weather conditions were: zero precipitation; sunny with varying cloud cover 1/8 – 6/8; air temperature 7 °C; winds west to south-west, 10 – 11.4 knots; wave calm to slight; Southampton neap tide predictions 05:39 +3.7m (high), 11:56 +1.8 m (low) and 18:35 +3.7 m (high).

Continuous depth readings were measured by the pressure-depth sensor on the Autonomous Benthic Recorder (ABR), which was triggered at 10:24 hours and took 2 minutes to deploy and to reach bed level at latitude 50° 46.413' N and longitude 001° 22.285' W. It was retrieved at 15:10 hours, and the data were extracted using the computer software Wave Log 19200 Baud. Twenty-two 512-second bursts of data files in MS Excel format were obtained from 10:24 to 15:06 hours. The first minute of the first data file was used to determine the average atmospheric pressure, which was found to be equivalent to 9.94 m of water (100.1 kPa ~ average atmospheric pressure at sea level). The pressure-depth sensor recorded total pressure (atmospheric + hydrostatic). To find the average hydrostatic pressure, the value of 100.1 kPa was subtracted from the average total pressure in each data file, giving an average water depth of approximately 5m. Before deployment, the height of the pressure-depth sensor was measured to be 0.45 m above the

base of the Valeport, so that figure was added to the average depth to get the time-averaged flow depth, h, at the investigation site. The first 2 minutes of the initial file were not used for further measurements as the ABR was deployed during this time.

The R.V. Bill Conway was moored approximately 20 m from the ABR at 50° 46.404¢ N 001° 22.280¢ W until 15:00 hours. At this position, temperature and salinity were measured at different depths and times using the Conductivity-Temperature-Depth instrument (CTD) for short periods between 10:35 and 14:34 hours. The CTD took Surface-to-bottom temperature and salinity profiles, as well as single measurements for surface, mid-depth, and bottom. Each set of measurements took from 3 – 5 minutes to obtain. The CTD measures the conductivity of the water, which is then converted into salinity on the Practical Salinity Scale.

Flow velocity and turbidity (as indicated by acoustic backscatter) at different depths and times were measured using the Acoustic Doppler Current Profiler (ADCP) from 10:13 to 14:58 hours, position 50° 46.404¢ N 001° 22.280° W. The data collected were extracted from the ADCP by the computer software WinRiver II and output as MS Excel files. Twenty-one velocity and backscatter profiles were computed using the measured depth values against time-averaged velocity and backscatter values. The profiles were arranged to correspond in time and duration to the data obtained from the ABR to make valid time comparisons. Because the ADCP was stopped at 14:58 hours, 12 minutes before the ABR was recovered at 15:10 hours, it was not possible to obtain the velocity and backscatter profile corresponding to the last ABR data file. However, twenty-one profiles collected from 10:26 to 14:53 hours, a duration of 4 hours 26 minutes, can be considered adequate to draw valid conclusions.

The ADCP measured flow velocity and backscatter at depths of intervals 0.5 m beginning from 1.79 m and ending at 4.79 m. However, because of the site's shallow flow depth (~ 5 m), many velocity and backscatter values at the 4.79 m depth were spurious as they were readings of either -32768 or blank cells. Therefore, the values at the 4.79 m depth were not used.

Bed shear stresses (BSS) were calculated using the velocity profile method involving the log-linear form of the von Karman-Prandtl equation, where κ is von Karman's constant :

$$\ln z = \frac{\kappa}{u_*} u(z) + \ln z_0 \qquad (1)$$

z = height of flow above the bed, u(z) = flow velocity at z, z0 = roughness length, u* = friction velocity, and κ = 0.4 (Dyer, 1986). This equation is derived from the exponential equation:

$$z = z_0 e^{\frac{\kappa u}{u^*}} \qquad (2)$$

Equation (2) gives the velocity profile shape in the water column.

The gradient of the log-linear graph of Equation (1) is κ/u*, from which u* was determined for each log-linear profile and used to calculate the corresponding bed shear stress, τ0:

$$\tau_0 = \rho u_*^2 \qquad (3)$$

where ρ = 1,027 kg/m3 (density of seawater). The graphing of Equation (1) was done in MS Excel, and the trend line equation and the coefficient of determination, R2, were computed to determine how closely the data points fit the log-linear form of Equation (1).

III. RESULTS

Of the twenty-one velocity profiles obtained from the ADCP, the first five did not exhibit the log-linear form of Equation (1), but diverged significantly from it, having $R^2 < 0.9$, while the remaining sixteen profiles conformed closely to the log-linear form. Table 1 summarizes these results along with the time intervals used for the ABR and ADCP and the state of the tide. Graphs of velocity against time and backscatter against time were plotted using the mid-interval time values.

ISSN No:-2456-2165

Table 1: Summary of ABR & ADCP time intervals used & velocity profile data.

Profile No.	From (hr)	To (hr)	Mid-interval (hr)	Velocity Profiles			
				R^2	Friction velocity u_* (m/s)	BSS τ_0 (N/m^2)	State of tide
0	10:26:37	10:33:23	10:30:00	0.382	-	-	ebb (slack)
1	10:37:52	10:46:23	10:42:07	0.231	-	-	ebb (slack)
2	10:50:52	10:59:23	10:55:07	0.822	-	-	ebb
3	11:03:52	11:12:23	11:08:07	0.002	-	-	ebb
4	11:16:52	11:25:23	11:21:07	0.702	-	-	ebb
5	11:29:52	11:38:23	11:34:07	0.997	0.046	2.18	ebb
6	11:42:52	11:51:23	11:47:07	0.995	0.057	3.37	low
7	11:55:52	12:04:23	12:00:07	0.983	0.028	0.81	flood
8	12:08:52	12:17:23	12:13:08	0.986	0.026	0.67	flood
9	12:21:52	12:30:23	12:26:08	0.986	0.027	0.74	flood
10	12:34:52	12:43:23	12:39:07	0.946	0.024	0.57	flood
11	12:47:52	12:56:23	12:52:08	0.988	0.025	0.66	flood
12	13:00:52	13:09:23	13:05:07	0.980	0.028	0.79	flood
13	13:13:52	13:22:23	13:18:07	0.897	0.026	0.68	flood
14	13:26:52	13:35:23	13:31:08	0.965	0.027	0.75	flood
15	13:39:52	13:48:23	13:44:08	0.959	0.027	0.75	flood
16	13:52:52	14:01:23	13:57:07	0.977	0.030	0.91	flood
17	14:05:52	14:14:23	14:10:07	0.945	0.017	0.29	flood
18	14:18:52	14:27:23	14:23:07	0.990	0.026	0.68	flood
19	14:31:52	14:40:23	14:36:07	0.996	0.027	0.75	flood
20	14:44:52	14:53:23	14:49:08	0.979	0.025	0.63	flood

The bed shear stress was high during 11:29-38 hours in the ebb tide just before the low tide. It reached the highest value at low tide, which levelled out to lower values ranging from 0.29 – 0.91 N/m2 for the flood tide. Shear stresses were not calculated for profiles 0 – 4 because the velocity profiles did not yield log-linear plots.

Figure 1a shows the partial tidal cycle obtained from the ABR pressure-depth data. In this partial cycle, the ebb tide occurred from 10:26 to 11:38 hours, the low tide from 11:42 to 11:51 hours and the flood tide from 11:55 to 14:53 hours. This is confirmed by the observed partial tidal data for Lymington (12 km west of the investigation site) for the same day and time, as shown in Figure 1b. Low tide at Lymington occurred from 11:26 to 11:36 hours, about 15 minutes earlier.

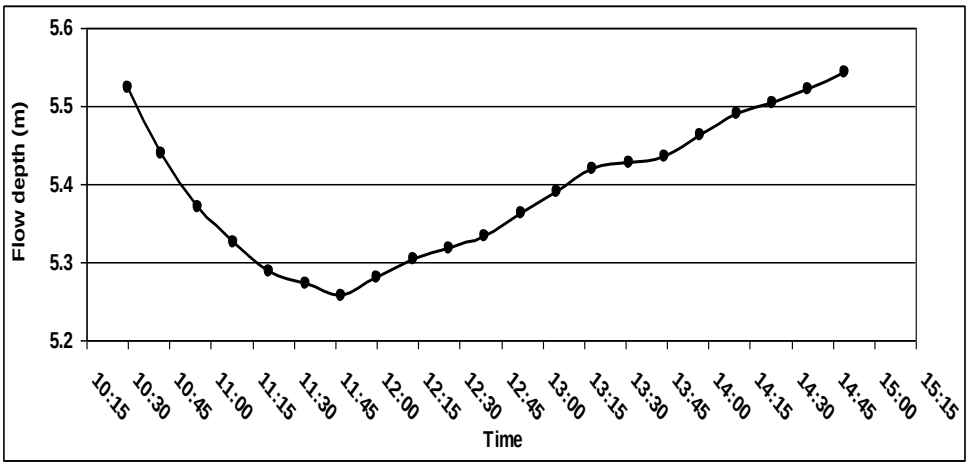

Fig. 1(a): The partial tidal cycle at the investigation site from 10:26 to 14:53 hours.

ISSN No:-2456-2165

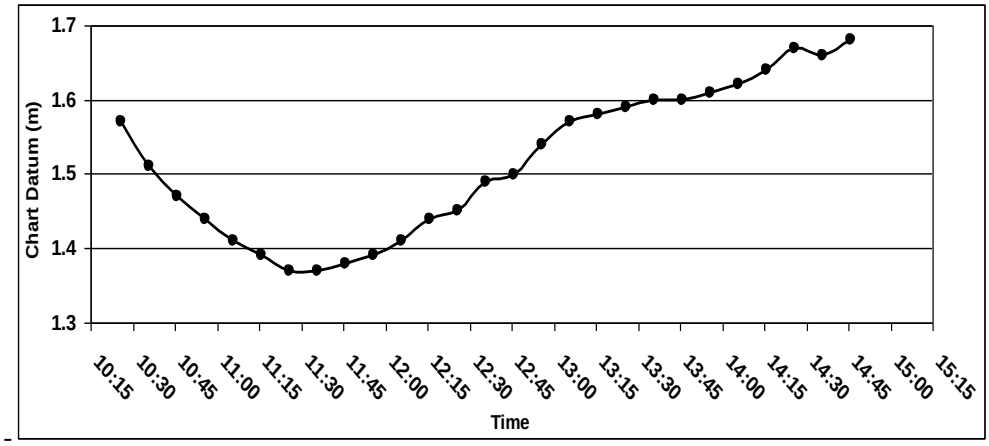

Fig. 1(b): The partial tidal cycle at Lymington from 10:26 to 14:46 hours.
(Channel Coastal Observatory, April 2009)

In Figures 2a – e on the next page, the velocity profiles are shown as flow depth vs. velocity. The profiles in Figures 2a & b occurred during the ebb tide and were significantly non-exponential, so it was not possible to extract log-linear plots from those profiles. The other ebb tide profiles showed similar features. Those occurring just before low tide and in the flood, for example, Figures 2c – e, closely conform to the characteristic exponential velocity profile that can be expressed in the log-linear form.

Figures 3a – e illustrates the corresponding backscatter profiles for Figures 2a – e. Backscatter was used as an indication of turbidity in the water column. During the ebb tide, turbidity increased with depth, and during the flood tide, turbidity decreased with depth.

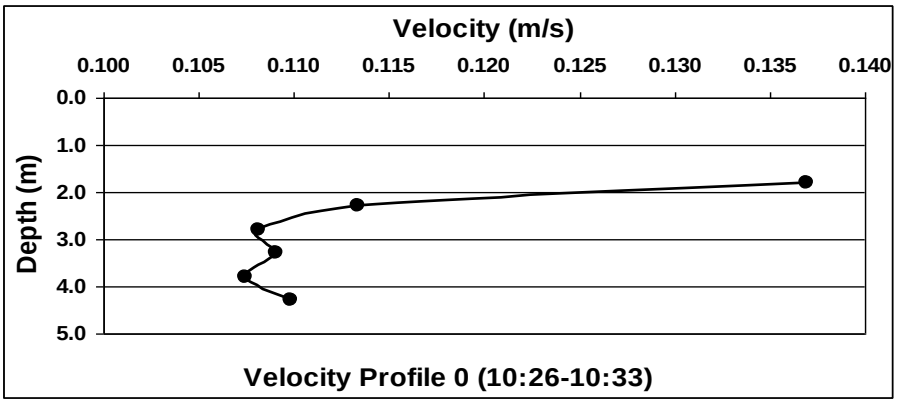

(a)

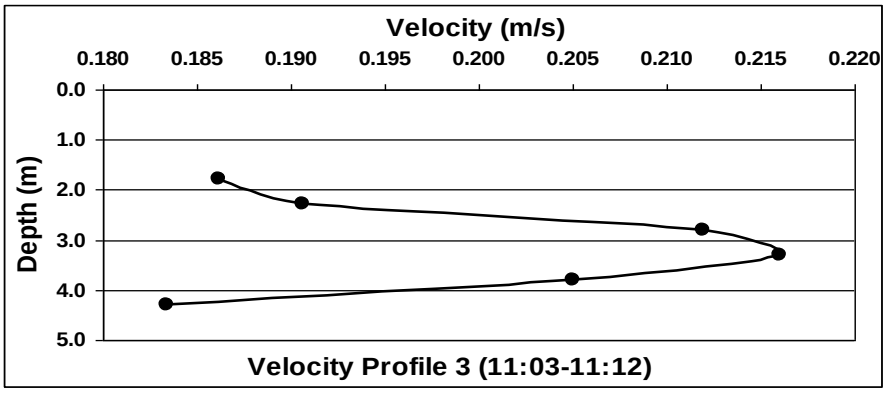

(b)

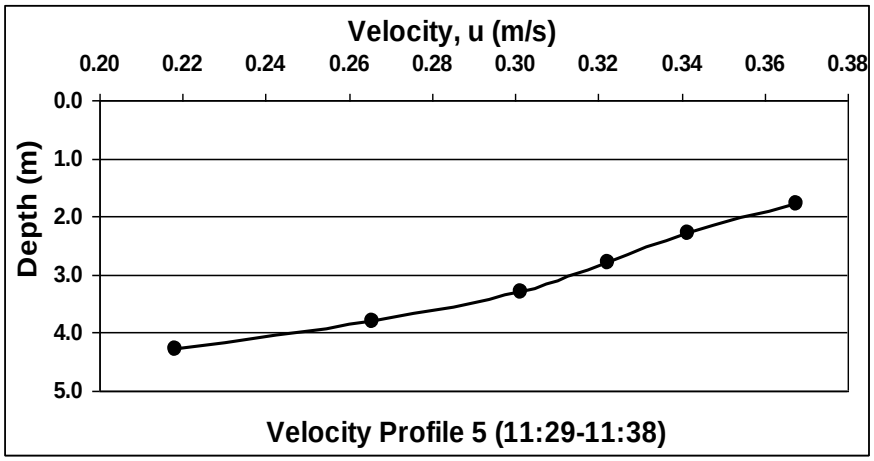

(c)

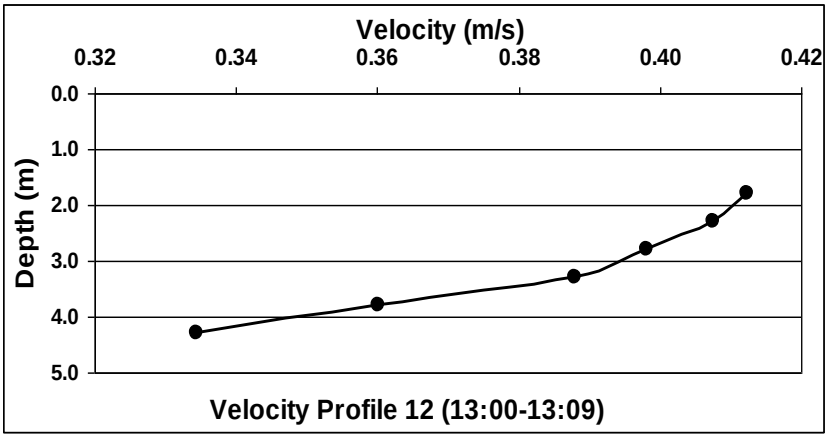

(d)

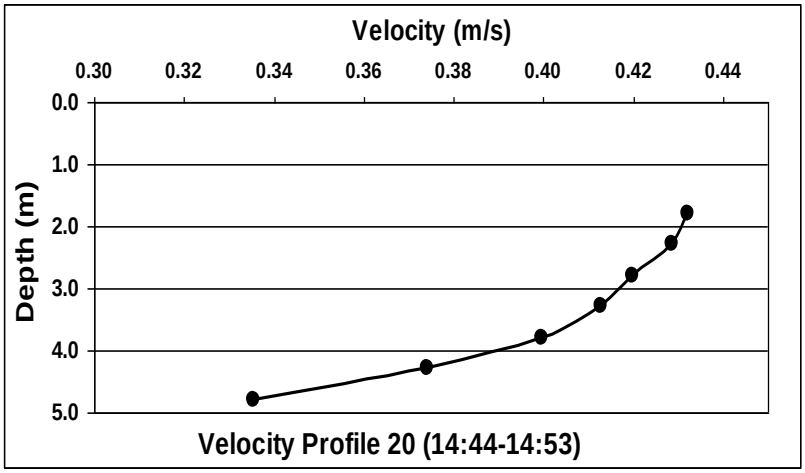

(e)

Fig. 2(a–e): Selected velocity profiles for five tidal times.

ISSN No:-2456-2165

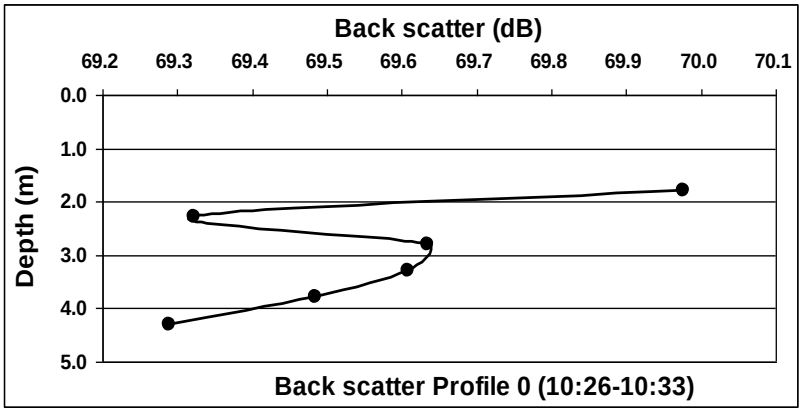

(a)

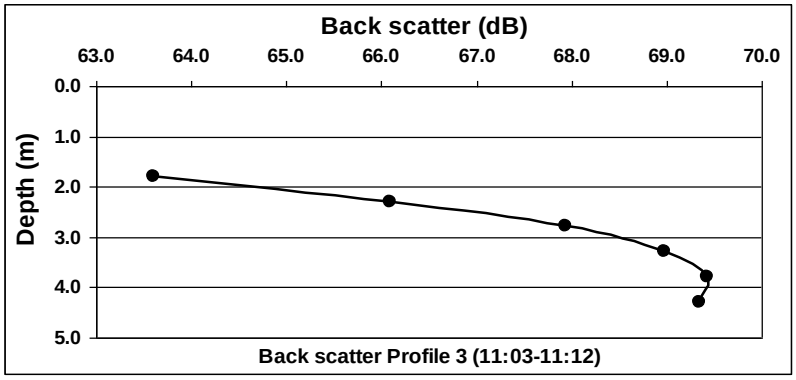

(b)

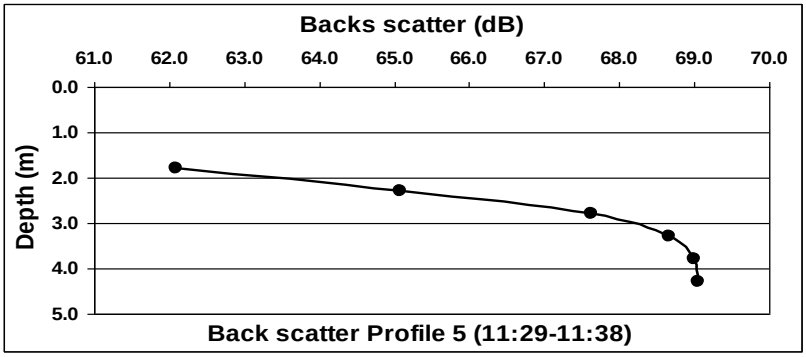

(c)

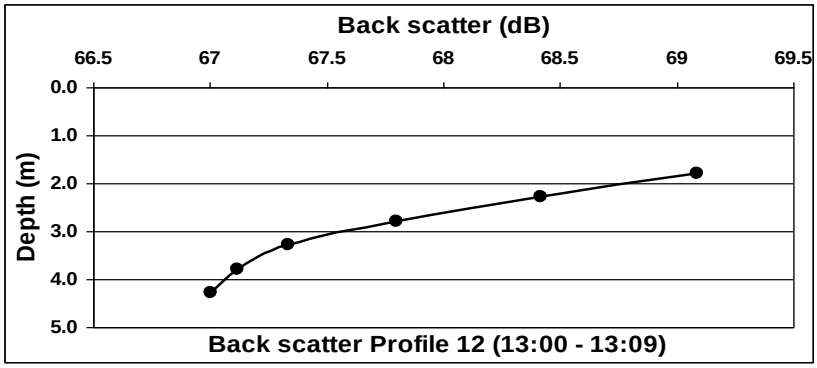

(d)

ISSN No:-2456-2165

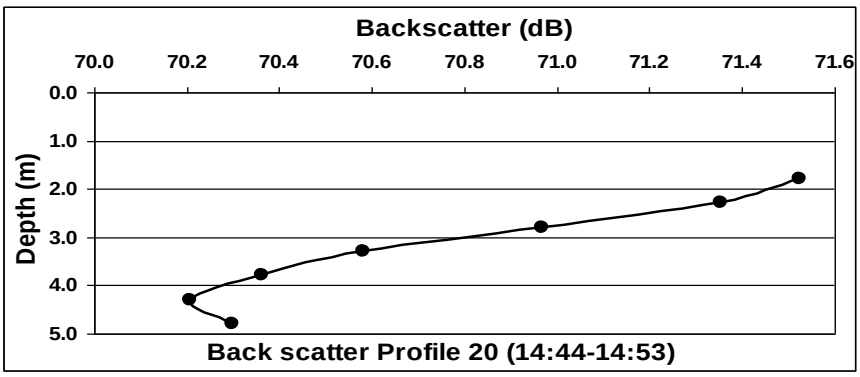

(e)

Fig. 3(a-e): Back scatter profiles for five tidal times.

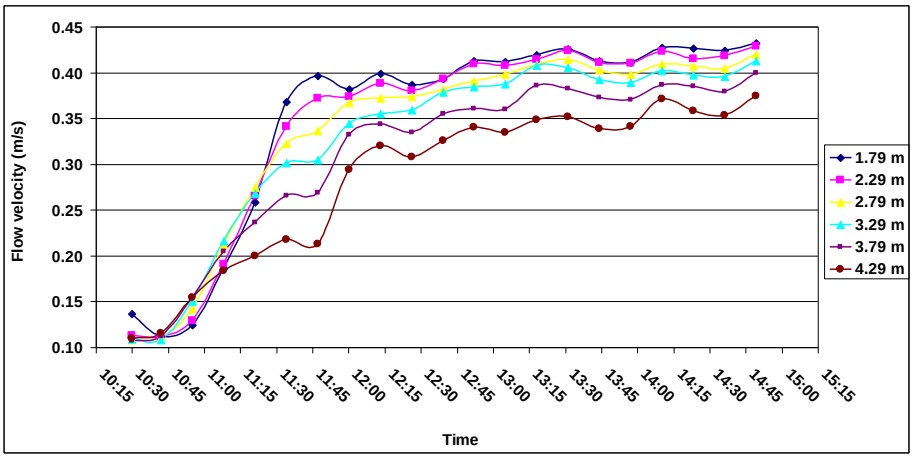

Fig. 4(a): Time-averaged flow velocities at six depths during the partial tidal cycle.

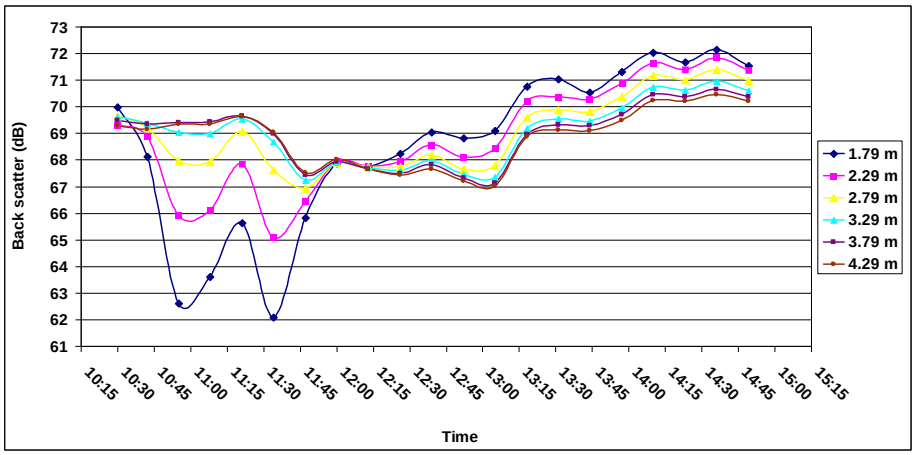

Fig. 4(b): Time-averaged back scatter at six depths during the partial tidal cycle.

Figure 4a shows that from 10:26 to 10:46 hours, the flow velocities at the six depths were lowest, ranging from 0.11-0.13 m/s, and were mixed. This was during slack water. Thereafter, the velocities increased as low tide approached, becoming more differentiated with respect to depth. By 11:30 hours, the velocities were fully differentiated, with faster velocities closer to the surface and slower velocities closer to the bed. From here, the velocity profiles began to attain the log-linear form. The flow continued to accelerate as low tide was reached at 11:42-11:51 hours. When the flood tide began at about 11:55 hours, the acceleration lessened, reaching maxima ranging from 0.43 m/s at the 1.79 m depth to 0.37 m/s at the 4.29 m depth. Figure 4b shows that during ebb, the backscatter is greater in flows closer to the bed, while during a flood, the backscatter is greater in flows closer to the surface. There is a sharp change-over of the back scatter-time plots when the flood fully begins by 12:00 hours.

ISSN No:-2456-2165

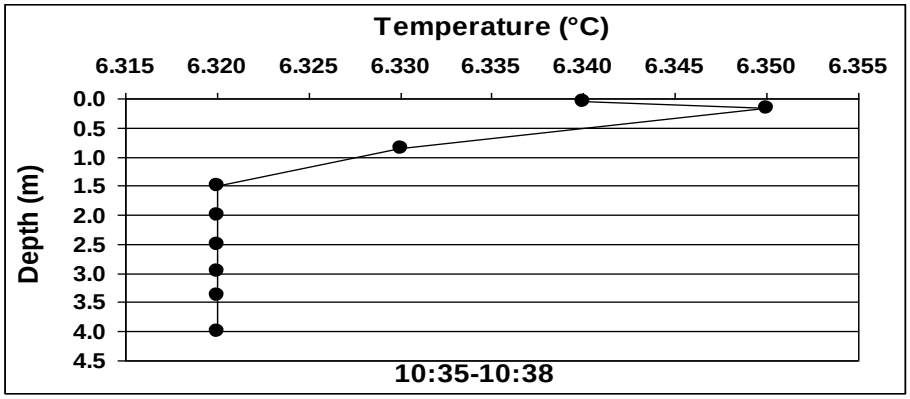

(a)

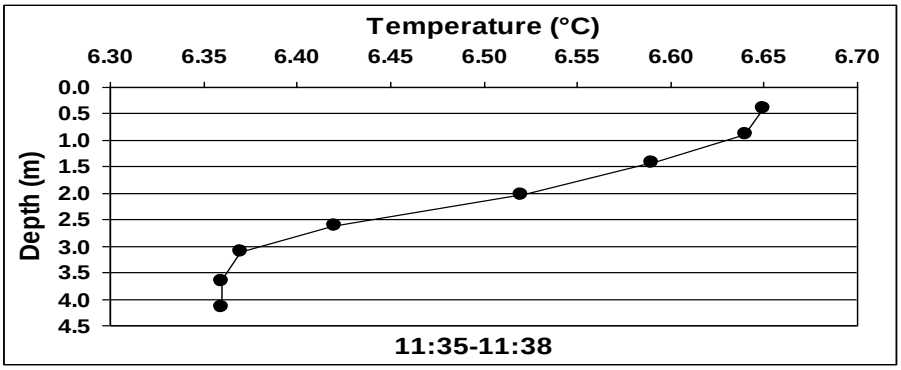

(b)

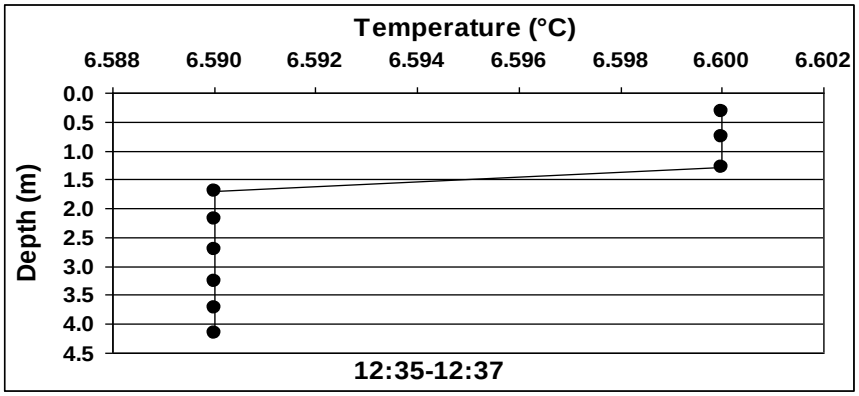

(c)

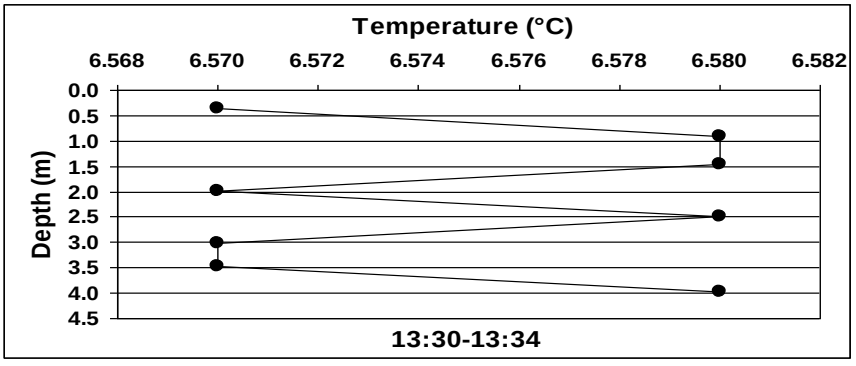

(d)

ISSN No:-2456-2165

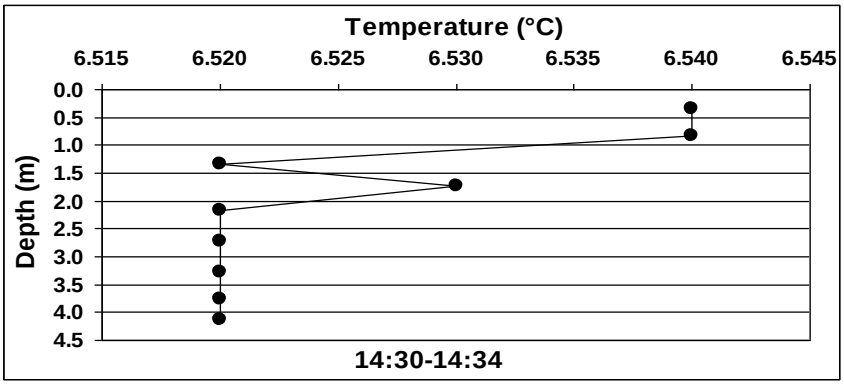

(e)

Fig. 5(a–e): Variations of temperature with depth at five tidal times

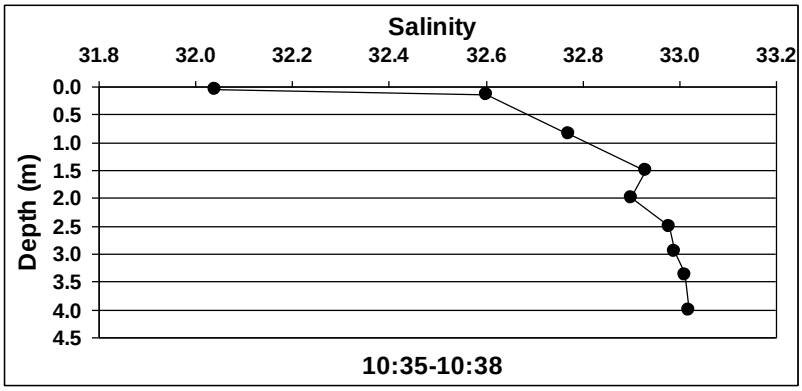

(a)

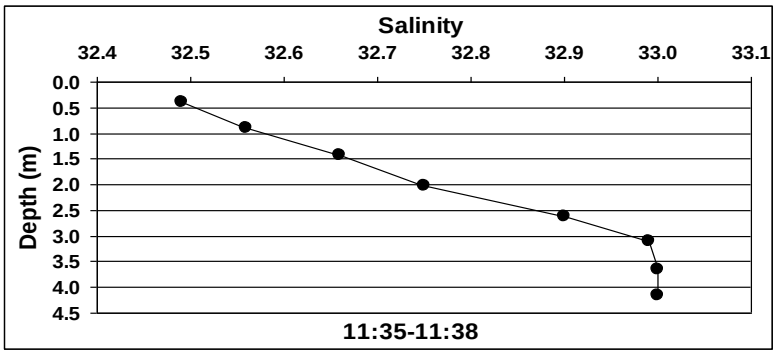

(b)

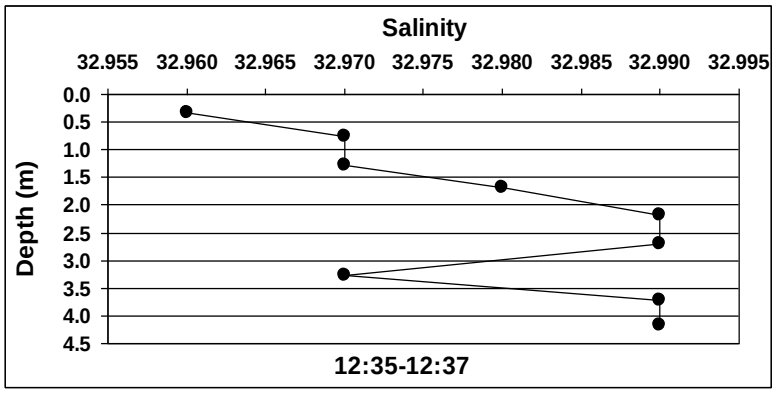

(c)

ISSN No:-2456-2165

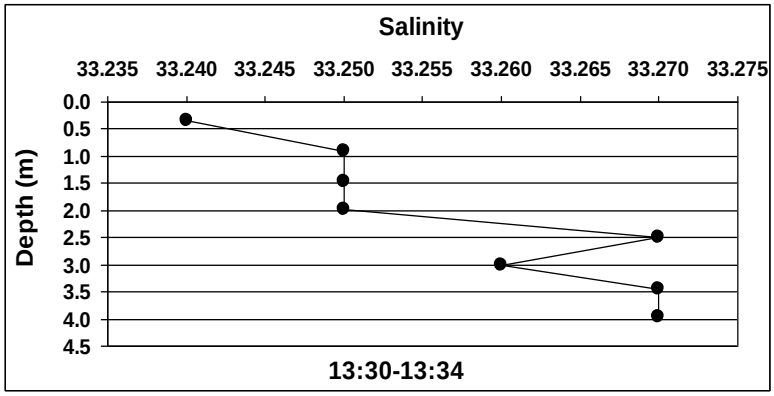

(d)

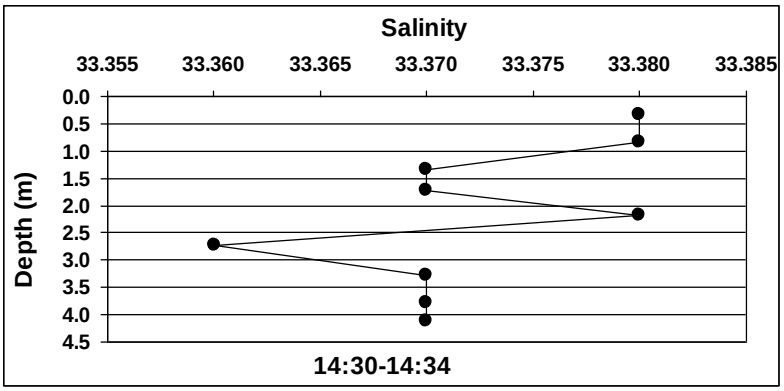

(e)

Fig. 6(a–e): Variations of salinity with depth at five tidal times

IV. DISCUSSION

During the ebb phase of the tidal cycle from 10:26 – 11:25 hours, no log-linear velocity profiles were observed because the state of the tide was slack water from 10:26-46 hours, followed by an acceleration of the flow from 10:50 – 11:25 hours. Flow velocities in the water column are minimal during slack water, and during an accelerated flow, velocities change rapidly over time. Both events will produce non-logarithmic velocity profiles since the formation of a logarithmic profile requires constant (or near-constant) flow uni-directional velocities at different depths, which implies zero (or minimal) acceleration, to produce a velocity profile of the shape expressed in Equations (1) and (2).

Logarithmic velocity profiles began to appear at 11:30 hours, just at the end of the ebb tide and lasted until the end of the investigation. This happened because the acceleration of the tidal flow lessened, and velocities leveled off at higher and constant (or near-constant) values, as shown in the velocity-time graph for different depths in Figure 4a. During the flood tide, the general observation is that water closer to the surface flows faster than water near the bed, with the flow velocity proportional to the logarithm of the height above the bed. This is in good agreement with the theory (Nielsen, 1992; Dyer, 1986; Yalin, 1972)

The minimal flow velocities during the slack water and ebb tide periods would ensure that the bed shear stresses would also be minimal, given that shear stress is proportional to the square of the flow velocity (Dyer, 1986).

During slack water and ebb tide, turbidity (as indicated by the acoustic backscatter) increased with depth, while during flood tide, turbidity decreased with depth (Figure 4b).

Since the flow velocities and bed shear stresses were minimal during the slack and ebb, the presence of near-bed suspended sediments causing the turbidity could not have been due to bed shear stress sending sediments into suspension. Instead, this was caused by sediments settling from higher up in the water column to lower down in the low-velocity, low-shear stress environment of slack water and the neap tidal ebb. During neap tides and ebb tides, the tidal forces and velocities are less than during spring tides and flood tides (Wood & Fleming, 1981; McDowell & O'Connor, 1977).

In the flood tide, the higher flow velocities produce higher bed shear stresses that send sediment into suspension higher up in the water column due to vertical turbulent mixing. This accounts for the observation that in the partial flood cycle from 12:00 – 14:53 hours, the backscatter (turbidity) is greater near the surface than near the bed because sediments have been

pushed toward the top of the water column by turbulence generated at the bed.

The temperature vs. depth profiles in Figures 5a – e show the general trend that the upper layers of water are warmer than the lower layers. Even though the temperature differences are small, ranging from 0.01°C (Fig. 1c & d) to 0.3 °C (Fig. 1b), the general trend is still evident.

The salinity vs. depth profiles in Figures 6a – e show the general trend that the denser, more saline water lies below the less dense, less saline water. The salinity differences between the different depths are small, ranging from 0.03 to 1. Generally, salinity increases with depth, while temperature decreases with depth. The denser, more saline water flows closer to the bed, and the less dense and warmer water flows closer to the surface. For both the temperature and salinity profiles, the differences are more pronounced during the ebb tide and less pronounced during the flood tide because, during the ebb, there is greater stratification of the water column than during the flood when more vertical mixing takes place (Kamphuis, 2000).

V. CONCLUSION

The investigation results confirm the temporal variation of the properties of the water column structure during the partial tidal cycle. These properties were turbidity, temperature, salinity, and flow velocity at different depths in the water column, which varied throughout the partial tidal cycle. There were variations across time (temporal) and variations across depths (spatial).

ACKNOWLEDGMENT

Thanks to Prof. Carl Amos and Dr. Charlotte Thompson of the University of Southampton, National Oceanography Centre, for advice and guidance.

Thanks also to the University for using the coastal vessel and laboratory facilities and providing the necessary technical support.

REFERENCES

[1.] Channel Coastal Observatory Realtime Tides Data. http://www.channelcoast.org/ April, 2009
[2.] Dyer, K. R. (1986). Coastal and Estuarine Sediment Dynamics, John Wiley & Sons Ltd., Chichester.
[3.] Dyer, K. R. (1973). Estuaries: A Physical Introduction, John Wiley & Sons Ltd., London.
[4.] Kamphuis, J. W. (2000). Introduction to Coastal Engineering, World Scientific Publishing Co. Pte. Ltd., Singapore.
[5.] McDowell, D. M. and O'Connor, B. A. (1977). Hydraulic Behaviour of Estuaries, The Macmillan Press Ltd., London.
[6.] Nielsen, P. (1992). Coastal Bottom Boundary Layers and Sediment Transport, World Scientific Publishing Co. Pte. Ltd., Singapore.
[7.] Oceanography Course Team. (1989). Seawater: Its Composition, Properties and Behaviour, Pergamon in association with the Open University, Oxford.
[8.] Open University Course Team. (1989). Waves, tides and shallow-water processes, Pergamon in association with The Open University, Oxford.
[9.] Wood, A. M. and Fleming, C. A. (1981). Coastal Hydraulics, The Macmillan Press Ltd., London.
[10.] Yalin, M.S. (1972). Mechanics of Sediment Transport. Pergamon Press Ltd., Oxford.